INTERFACE FOCUS

royalsocietypublishing.org/journal/rsfs

Review

Cite this article: Tostevin R, Mills BJW. 2020 Reconciling proxy records and models of Earth's oxygenation during the Neoproterozoic and Palaeozoic. *Interface Focus* **10**: 20190137.
http://dx.doi.org/10.1098/rsfs.2019.0137

Accepted: 20 April 2020

One contribution of 15 to a theme issue 'The origin and rise of complex life: integrating models, geochemical and palaeontological data'.

Subject Areas:
biogeochemistry

Keywords:
Neoproterozoic, Palaeozoic, oxygenation, redox proxies, COPSE

Author for correspondence:
Rosalie Tostevin
e-mail: rosalie.tostevin@uct.ac.za

Electronic supplementary material is available online at https://doi.org/10.6084/m9.figshare.c.4966277.

THE ROYAL SOCIETY PUBLISHING

Reconciling proxy records and models of Earth's oxygenation during the Neoproterozoic and Palaeozoic

Rosalie Tostevin[1] and Benjamin J. W. Mills[2]

[1]Department of Geological Sciences, University of Cape Town, Rondebosch, Cape Town, South Africa
[2]School of Earth and Environment, University of Leeds, Leeds LS2 9JT, UK

RT, 0000-0003-2843-7741

A hypothesized rise in oxygen levels in the Neoproterozoic, dubbed the Neoproterozoic Oxygenation Event, has been repeatedly linked to the origin and rise of animal life. However, a new body of work has emerged over the past decade that questions this narrative. We explore available proxy records of atmospheric and marine oxygenation and, considering the unique systematics of each geochemical system, attempt to reconcile the data. We also present new results from a comprehensive COPSE biogeochemical model that combines several recent additions, to create a continuous model record from 850 to 250 Ma. We conclude that oxygen levels were intermediate across the Ediacaran and early Palaeozoic, and highly dynamic. Stable, modern-like conditions were not reached until the Late Palaeozoic. We therefore propose that the terms Neoproterozoic Oxygenation Window and Palaeozoic Oxygenation Event are more appropriate descriptors of the rise of oxygen in Earth's atmosphere and oceans.

1. Introduction

Since the Great Oxidation Event, 2.5–2.3 billion years ago (Ga), oxygen has been a persistent feature of Earth's atmosphere [1], but has remained at low levels throughout the Palaeoproterozoic and Mesoproterozoic eras (2.5–1.0 Ga). A hypothesized rise towards modern oxygen levels in the Neoproterozoic (1.0–0.54 Ga) was dubbed the 'Neoproterozoic Oxygenation Event' (NOE) [2]. Evidence for the NOE included broad increases in the average molybdenum and vanadium concentrations in black shales [3]; an increase in the isotope fractionation between sulfate and pyrite ($\Delta^{34}S_{SO4-pyr}$) [4]; and Fe speciation evidence for local deep water oxygenation [5].

Geochemical data collected over the last decade have disrupted this narrative. Despite an increase in the breadth and depth of proxy data now available, we appear to be further from a consensus on the timing and dynamics of oxygenation. Some proxies support a single, unidirectional step change in oxygen levels, although the estimates of the timing span almost 600 Myr [6–15]. Other proxy data support a more dynamic system, with large oscillations in oxygen availability [16–18].

How can we reconcile these different proxy records? One possibility is that some of the geochemical data do not record ancient redox conditions, because they have been overprinted by diagenesis and metamorphism. While some published data may need to be revisited, other geochemical signals are reproducible in samples from different basins (e.g. uranium isotopes [18,19] or redox sensitive trace elements [7,17,20,21]). In addition, geochemical redox analysis can be paired with petrography or other geochemical data to screen for potential alteration. Another possibility is that we are misinterpreting primary geochemical signals. Because today's oceans are largely well-oxygenated, proxy systems are calibrated in isolated basins and lakes, and these environments may not provide a reasonable analogue for a globally anoxic deep ocean. Alternatively, each proxy may be capturing different parts of a complex transition, depending on the

proxy systematics, marine residence time, reduction potential and sampling density. Here, we critically evaluate current proxy evidence for Neoproterozoic–Palaeozoic oxygenation, attempt to reconcile the various records and compare them to the latest biogeochemical modelling results.

2. Evaluation of current geochemical evidence

2.1. Local marine geochemical proxies

Local marine redox proxies record progressive changes within a single basin [5,22], but if those changes are driven by local hydrodynamics or changes in productivity, they may not reflect global changes in oxygen availability. When sufficient local proxy data are collected from multiple basins, the compiled data may record a statistically significant change in the average oxidation state of the ocean. However, these proxy records are necessarily biased towards shelf and slope environments, as Proterozoic sediments from the abyssal plain are rarely preserved. Proxies preserved in carbonates, such as I/Ca and Ce anomalies, are further biased towards warm, shallow shelf environments at low latitudes.

2.1.1. Iron speciation

The ratio of highly reactive to total iron preserved in carbonates and shales is indicative of the redox chemistry in the water column directly above the accumulating sediments [23]. Robust calibrations of the proxy in modern sediments allow the differentiation of oxic ($Fe_{HR}/Fe_T < 0.22$) and anoxic water masses ($Fe_{HR}/Fe_T > 0.38$), although ambiguous ratios may be generated under high sedimentation or mixing rates (Fe_{HR}/Fe_T 0.22–0.38). For anoxic water masses, the proportion of pyrite in the highly reactive iron phase can distinguish between Fe-bearing (ferruginous) and sulfidic (euxinic) anoxia (table 1). Therefore, 'oxic' conditions identified by iron speciation could potentially incorporate suboxic and well-oxygenated conditions. Systematic diagenetic biases could be introduced to the iron speciation record through transformation of unsulfidized highly reactive iron minerals to less reactive sheet silicates, producing a false oxic signal.

A transition towards oxic Fe speciation signals approximately 580 Ma, recorded in shales deposited on a continental slope, was thought to pinpoint permanent oxygenation of the deep ocean [5]. However, as more data have been collected, an increasingly complex picture of spatial and temporal heterogeneity has emerged. For example, data from basins of the same age in the Canadian cordillera show no such oxygenation [21,24], and younger basins record anoxic waters impinging onto the shelf [25]. A recent statistical analysis of 4700 Fe speciation measurements from deep water settings across a range of ages and locations has revealed no significant long-term (i.e. 100 Myr) trend towards more oxic conditions across the Neoproterozoic and early Palaeozoic (figures 1 and 2) [14]. This study has good spatial and temporal coverage from approximately 2.1 Ga to 440 Ma, although Silurian–Devonian data come from just two studies and may be subject to sampling biases (figure 2) [7,32].

2.1.2. Iodine to calcium ratios

Iodine to calcium ratios in carbonate rocks reflect local water column redox conditions. Since the reduction of iodate (IO_3^-) to iodide (I^-) has a relatively high reduction potential, the I/Ca proxy is sensitive to intermediate redox conditions, from hypoxic (less than 70–100 µM O_2) to suboxic (manganous–nitrogenous conditions) [33] (table 1). Iodate is incorporated into carbonate rocks, and so I/Ca ratios reflect the oxidized iodate concentration in the local water column at the depth of carbonate formation, which varies with the concentration of oxygen in surface waters and the depth of the top of the oxygen minimum zone (OMZ) [10]. Due to the slow kinetics of iodide oxidation, water masses with fluctuating redox conditions, or anoxia nearby, may retain a low iodate signature, biasing primary signatures towards anoxic conditions. In addition, diagenesis can reduce the I/Ca ratio, but not increase it, systematically biasing the rock record towards anoxic conditions [26].

I/Ca data span a large range at any given location, but if there are sufficient data, then an increase in the maximum I/Ca may indicate oxygenation. Long-term compilations reveal variable but low I/Ca across the Neoproterozoic and Early Palaeozoic [26] (figure 2), with notable peaks during the Bitter Springs (approx. 810–800 Ma) [28] and the Shuram excursion (approx. 560 Ma) [26,34]. I/Ca ratios show a significant peak in the Devonian, between approximately 400 and approximately 350 Ma, but a return to lower values in the Carboniferous and Permian (figures 1 and 2) [10]. There is no permanent change towards higher I/Ca ratios until the early Mesozoic. The maximum I/Ca recorded in any given time window may evolve as more data are collected.

2.1.3. Cerium anomalies

Negative Ce anomalies in rare earth element patterns are indicative of locally oxic water column conditions. Under oxidizing conditions, Ce(III) is oxidized to Ce(IV) on the surface of Mn (oxyhydr)oxide minerals, resulting in relative depletion in shale-normalized seawater Ce concentrations compared with the other rare earth elements. The generation of Ce anomalies requires oxidation of Mn and Ce, both of which have relatively high reduction potentials (+1.23 mV and +1.44 mV, respectively). Therefore, Ce anomalies are responsive to the onset of manganous conditions, which may overlap with low oxygen concentrations (less than 10 µM). Ce anomalies can respond to redox changes over metre scales [35], although in the open ocean, local signals may be overprinted by basin-wide signals due to slow kinetics [29] (table 1). The magnitude of any Ce anomaly may correspond to the concentration of oxygen or the thickness of the oxic layer, but can also be influenced by other factors such as local Mn oxide fluxes [36]. Rare earth elements, and associated Ce anomalies, substitute for Ca^{2+} in the carbonate mineral lattice, and as such, can faithfully record seawater rare earth elements at the site of carbonate formation and are relatively robust to diagenesis and even dolomitization [30,37].

A progressive increase in the magnitude of the Ce anomaly after 551 Ma in carbonate rocks from South China was interpreted to record an increase in oxygen levels in the shallow marine environment during the late Ediacaran [22]. However, reducing signals have since been recorded in contemporaneous rocks from the Nama Group, Namibia [31], suggesting oxygenation was not a global phenomenon. Further, long-term compilations of Ce anomaly data from 18 formations show no significant change until the Late Devonian (approx. 383 Ma; figures 1 and 2) [29]. However, this broad compilation includes large sample gaps. For example, there is only one sample between approximately 600 Ma and approximately 550 Ma.

Table 1. Summary of proxy systematics.

	proxy	responds to	redox sensitivity	archives	systematic bias?
local/regional marine	iron speciation	integrated regional water column redox conditions above accumulating sediments	ferruginous anoxia and euxinia	shales, carbonate	variable
	I/Ca ratios	upper ocean oxygen gradients	hypoxic (<70 µM O_2) to suboxic (between manganous and nitrogenous)	carbonates	false anoxic
	Ce anomalies	local–regional water column redox at site of carbonate precipitation	suboxic (manganous)	carbonates, phosphorites, iron formation	false anoxic
	$\sum Fe^{3+}/Fe$	regional deep water oxygen concentrations	progressive with increasing $O_2(aq)$	basalts	false anoxic
	marine red beds	regional deep ocean oxygen concentrations following periods of anoxia	ferruginous anoxia	marine red beds	
global marine	$\delta^{238}U$	area of global seafloor bathed in anoxic waters	anoxia	carbonates, shales	false oxic
	$\delta^{98}Mo$	area of global seafloor bathed in anoxic waters	euxinia	shales	false anoxic
	RSE enrichments	area of global seafloor bathed in anoxic waters	euxinia (Mo); ferruginous anoxia (Cr, Re, U, V)	euxinic shales	false anoxic
	$\delta^{82}Se$	local redox conditions and size of global–regional oxidized SeO_x^{2-} reservoir	ferruginous anoxia	shales	
	$\delta^{34}S$	size of global marine sulfate reservoir and global proportional pyrite burial flux	euxinia, atmospheric O_2	carbonates, evaporites	variable
atmospheric	$\delta^{53}Cr$	atmospheric oxygen	>0.1–1% PAL	shales, ironstones	
	wildfire record	atmospheric oxygen	>70% PAL	charcoal	

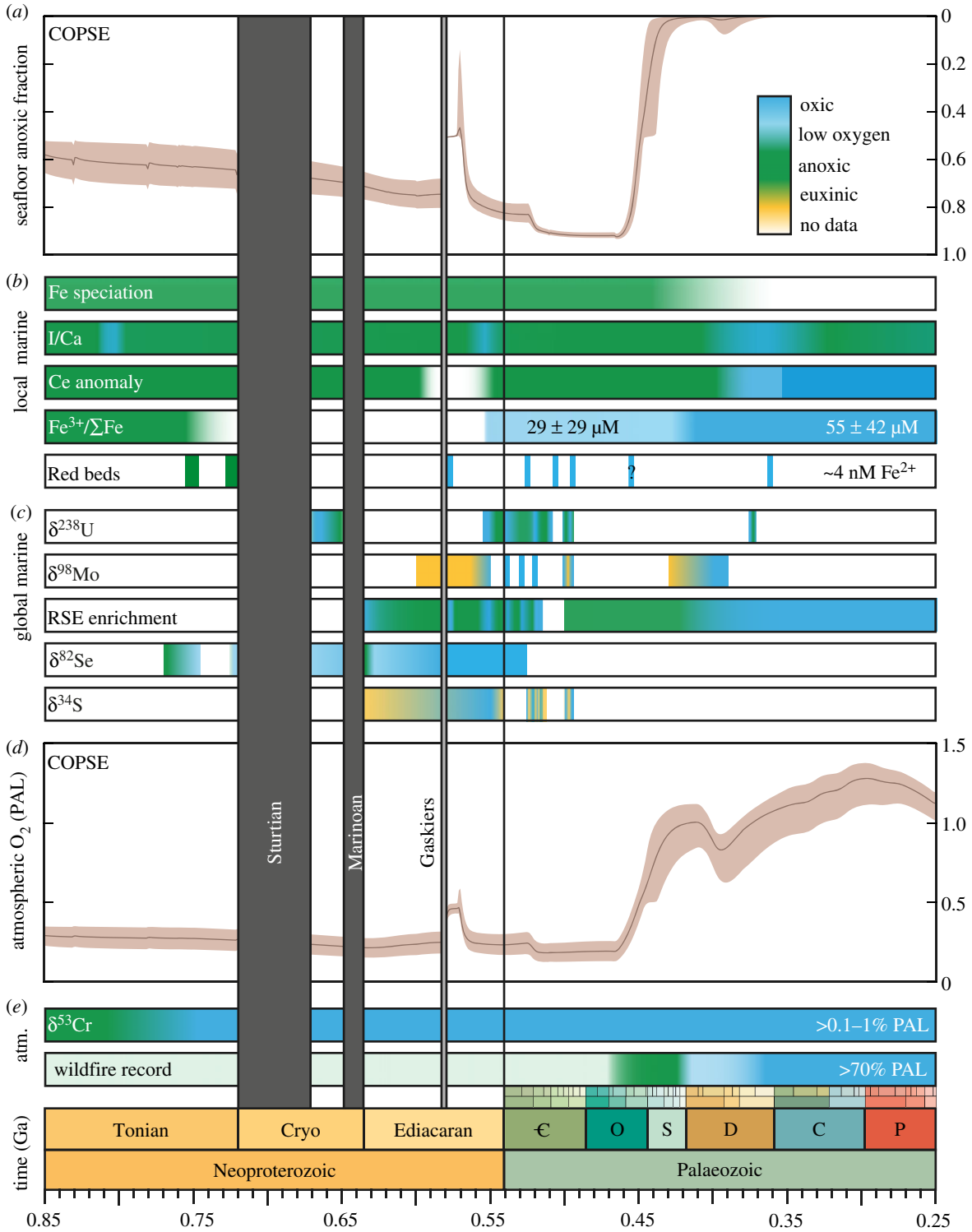

Figure 1. COPSE model predictions of atmospheric and marine redox and inferred redox conditions based on geochemical proxies through the Neoproterozoic and Palaeozoic. (*a*) Modelled seafloor anoxia. Shaded area shows bounds of 10 000 sensitivity analyses. (*b*) Proxy inferences for local marine oxygenation, indicating dominantly euxinic (yellow), anoxic (green), low oxygen (light blue) and oxic (dark blue) conditions. Surface waters have contained some oxygen since the GOE, but these interpretations represent the dominant redox conditions. Therefore, a green bar does not imply that the entire ocean was anoxic. For interpretation of each dataset and relevant references, see discussion in the text. (*c*) Proxy inferences for global marine oxygenation. (*d*) Modelled atmospheric O_2 (PAL). (*e*) Proxy inferences for atmospheric O_2.

2.1.4. $Fe^{3+}/\sum Fe$ ratio of submarine basalts

As oxygenated water circulates through seafloor basalts, reduced iron is oxidized to Fe^{3+}. Therefore, the $Fe^{3+}/\sum Fe$ ratio of submarine basalts varies with the magnitude of hydrothermal fluxes and with the oxygen content of bottom waters. As such, seafloor basalts, preserved as ophiolites, can provide a direct record of deep water oxygen concentrations (table 1). Metamorphism acts to reduce Fe^{3+} and so could systematically bias the $Fe^{3+}/\sum Fe$ ratio towards lower values.

Long-term compilations of $Fe^{3+}/\sum Fe$ data show no significant change across the Archean and Proterozoic (Archean = 0.20 ± 0.04; Palaeo–Mesoproterozoic = 0.26 ± 0.02; Neoproterozoic = 0.26 ± 0.05), but a progressive increase across the Early Palaeozoic (0.34 ± 0.08), Late Palaeozoic (0.47 ± 0.10) and Mesozoic–Cenozoic (0.58 ± 0.11) (figure 2) [15]. This indicates a progressive increase in oxygen content of the deep ocean from 11 ± 17 µmol kg^{-1} in the Neoproterozoic, to 29 ± 29 µmol kg^{-1} in the Early Palaeozoic, 55 ± 42 µmol kg^{-1} in the

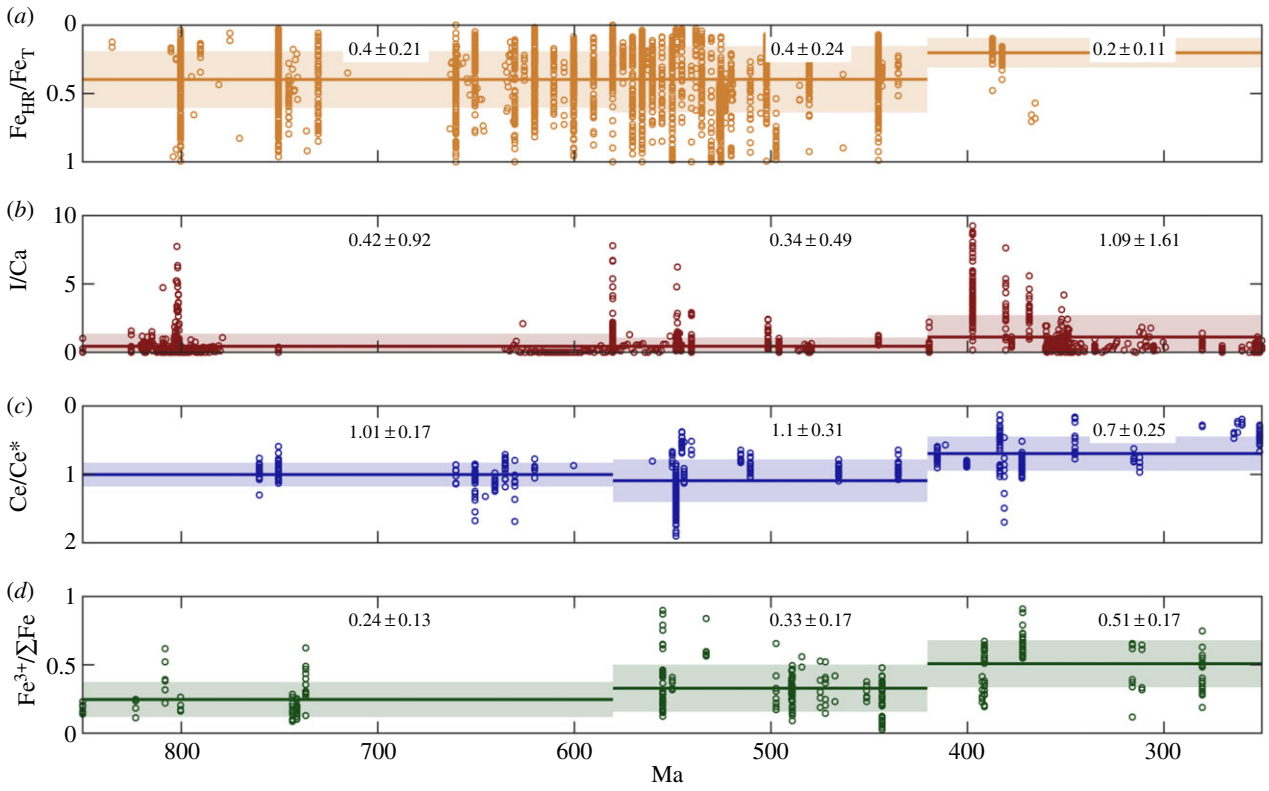

Figure 2. Geochemical data for local–regional redox proxies from 850 to 250 Ma. Data (open circles) for Fe speciation from shales [14], I/Ca ratios in carbonate rocks [10,26–28], Ce anomalies in carbonate rocks [29–31] and $Fe^{3+}/\sum Fe$ ratios of seafloor basalts [15]. The average (solid line) and an error window of 1 standard deviation (shaded region) are shown for time bins 850–580, 580–420 and 420–250 Ma.

Late Palaeozoic and 80 ± 53 µmol kg^{-1} in the Mesozoic–Cenozoic (figure 1). Due to the distribution of rare ophiolites in the geological record, there are large gaps where no data are available, as well as large uncertainties in the age of some samples. For example, there are no data between 736 ± 1.7 Ma and 554.5 ± 136.5 Ma. In the Stolper & Keller [15] study, the Neoproterozoic time bin is dominated by samples greater than 700 Ma, but samples between 555 and 541 are within range of the Early Palaeozoic average (this is reflected in figure 1).

2.1.5. Red beds

The distribution of iron rich rocks through the geological record may reflect ocean redox dynamics and Fe^{2+} concentrations [13]. Iron formation requires Fe^{2+} concentrations greater than 50 µM, whereas marine red beds, which are thinner and have lower % Fe, only require greater than 4 nM. Major periods of marine red bed deposition occurred in the mid-Ediacaran, Cambrian and Late Devonian, with a possible event in the late Silurian [13] (blue on figure 1). These sporadic events indicate lower deep water Fe concentrations following anoxic events, which could be consistent with more oxygenated deep oceans. This record is biased towards preserved shelf sediments and may evolve if more examples are documented.

2.2. Global marine geochemical proxies

2.2.1. Uranium isotopes

The uranium isotope ratio of seawater ($\delta^{238}U$) is sensitive to the global proportion of seafloor overlain by anoxic bottom waters. During reduction of soluble U(VI) to insoluble U(IV) under anoxic conditions, sedimentary U(IV) is enriched in ^{238}U, leaving seawater depleted in ^{238}U. Therefore, when the anoxic sink expands, seawater $\delta^{238}U$ decreases, and this signal can be preserved in carbonates. Organic-rich mudrocks also track changes in seawater $\delta^{238}U$, but the signal is offset by a variable local fractionation factor [38] (table 1). $\delta^{238}U$ data can be used to calculate the proportion of anoxic seafloor, although these estimates rely on several calibration factors that were determined in modern lakes (e.g. the Black Sea [39]). In particular, the calculations are sensitive to the isotope fractionation during U reduction, but more work is needed to explore how this varies under euxinic and anoxic ferruginous conditions. Above approximately 20% seafloor anoxia, the proxy begins to saturate [40], and large changes in the proportion of seafloor anoxia only translate into small changes in $\delta^{238}U$. These small changes are within the error introduced by diagenesis [41], which can result in positive $\delta^{238}U$ offsets of less than 0.3‰.

Uranium isotope data are available for parts of the Neoproterozoic–Cambrian record (the post-Sturtian interval, and approximately 560 to approximately 510 Ma). These data show large oscillations between high, modern-like $\delta^{238}U$, and very low $\delta^{238}U$, suggesting that long-term anoxia was punctuated by ocean oxygenation events at approximately 660, 560, 540 and 520 Ma (figure 1) [9,18,19,40,42,43]. Some of these oscillations are confirmed by multiple studies in different basins [9,18,19]. Short-term switches towards anoxic conditions are recorded approximately 497 Ma [44] and 372 Ma [45]. Placing $\delta^{238}U$ into a quantitative model suggests seafloor anoxia oscillated from greater than 30% during periods of quiescence, to less than 1% during oxygenation events [18].

2.2.2. Molybdenum isotopes

High $\delta^{98}Mo$ values preserved in shales indicate globally widespread oxic conditions, under which large negative isotope

fractionations occur during adsorption of Mo onto Mn oxides, leaving seawater isotopically enriched (table 1). By contrast, under euxinic conditions, Mo is rapidly and quantitatively removed. Since all known sedimentary Mo sinks have a δ^{98}Mo below contemporaneous seawater, δ^{98}Mo measurements only provide a minimum constraint on $\delta^{98}Mo_{SW}$. Further, interpretations of sedimentary δ^{98}Mo rely on independent proxy evidence for local redox conditions. Changes in δ^{98}Mo could also result from a switch from euxinic to ferruginous anoxia, with no overall increase in oxygenated waters.

Pulses in δ^{98}Mo are recorded between 550 and 520 Ma, each one reaching progressively higher δ^{98}Mo maxima [6]. This was interpreted to indicate progressive marine oxygenation across the Cambrian, but the data contain a lot of scatter and could also be consistent with discrete oxygenation pulses at approximately 552, 540, 530 and 521 Ma (figure 1) [6,7,9]. Distinguishing between these two scenarios is difficult because the rarity of black shales deposited under fully euxinic conditions limits the resolution of the record. The magnitude of δ^{98}Mo enrichments increases through time, suggesting each oxygenation event was more significant than the last [6]. δ^{98}Mo reaches stable, modern-like levels between the mid-Silurian and mid-Devonian (approx. 430–390 Ma) [7]. Modelling calculations suggest that oxygenation events in the Neoproterozoic were limited (33% oxic seafloor) [6,7], but reached greater than 97% oxic seafloor by approximately 520 Ma, although many of the parameters in these models are poorly constrained.

2.2.3. Redox sensitive elements

Because Mo is scavenged from seawater under euxinic conditions, and V, U, Re and Cr are scavenged under ferruginous conditions, an increase in the concentration of redox sensitive elements (RSE) in seawater can indicate the global retreat of anoxic sinks. RSE concentrations in shales are controlled by the size of the global RSE reservoir and an enrichment factor, which varies with the local redox conditions. RSE concentrations are commonly analysed in sediments where there is independent evidence for local euxinia, to ensure a consistent local enrichment factor, meaning any enrichments in RSE can be attributed to an expanded global marine RSE reservoir (table 1). RSE data typically show large amounts of scatter, but an increase in the average or maximum concentration can be interpreted as evidence for an increase in the area of oxic seafloor.

Long-term compilations appeared to show an abrupt increase in Mo, V and U concentrations between 663 and 551 Ma [3,46], interpreted to mark widespread oxygenation of the oceans [2]. A recent re-analysis of the U record shows that there is a statistically significant increase in average U concentrations between the Cambrian–Silurian and Devonian–Permian, suggesting any step change towards more permanently oxygenated oceans occurred in the Palaeozoic (figure 1) [14,46]. The precise timing of any change will depend on the positions of relatively long time-scale bins used for data analysis. However, a more complete stratigraphic record with higher sampling density, from a demonstrably open ocean section in Wuhe, South China, has revealed pulses of RSE enrichment at regular intervals, representing ocean oxygenation events at 635, 580, 560, 540, 530 and 522 Ma (figure 1) [17]. Similar enrichments are observed in other sections located on different cratons, suggesting a truly global signal [7,20,21]. In between these oxygenation events, the widespread anoxia that characterizes much of the Proterozoic returns. Modelling efforts suggest that relatively limited seafloor euxinia (1–10%) and more extensive seafloor anoxia (greater than 30–40%) are needed to crash the global Mo and Cr reservoirs, respectively [47].

2.2.4. Selenium isotopes

Se isotopes (δ^{82}Se) in marine shales are a novel tracer for ocean–atmosphere oxygenation. Se has a reduction potential between S(–II)/S(IV) and Fe(III)/Fe(II) and a relatively short marine residence time (1100–26 000 years) [48]. During oxyanion (SeO_x^{2-}) reduction under anoxic conditions, isotopically light Se is sequestered into the sediments, driving surface waters isotopically heavy. In addition, an increase in the size of the SeO_x^{2-} reservoir correlates with larger fractionations in locally suboxic sediments (table 1). Sediments deposited in oxic open oceans, or below well-connected OMZs, have lower δ^{82}Se than those from restricted anoxic basins, due to the larger SeO_x^{2-} reservoir. δ^{82}Se yields insight into the local water column redox conditions, with an additional global control. The signal may be further complicated by variations in riverine input, locally enhanced productivity, or basin restriction.

A progressive decrease in δ^{82}Se is recorded in shales across the Ediacaran, reaching a minimum around the end of the Ediacaran [12]. For the pre-Gaskiers record, the signal is confirmed in multiple sections, suggesting a global control. This is probably a reflection of an increasing SeO_x^{2-} reservoir, which could reflect ocean oxygenation. Overall, the record is difficult to interpret, but suggests a slow but steady shift from fully anoxic to fully oxic deep waters between 750 and 540 Ma.

2.2.5. Sulfur isotopes

Under euxinic conditions, microbial sulfate reduction converts sulfate (SO_4^{2-}) into sulfide (HS^-), which may be buried as pyrite. The δ^{34}S of seawater sulfate is sensitive to the global pyrite burial flux, and the isotope fractionation associated with that pyrite burial. Both of these parameters are closely tied to ocean–atmosphere redox (table 1). The δ^{34}S signature of seawater is complex [49], but higher $\delta^{34}S_{SO4}$ could indicate enhanced pyrite burial, which may be driven by expanded euxinia. Large offsets between $\delta^{34}S_{SO4}$ and $\delta^{34}S_{pyr}$ ($\Delta^{34}S_{SO4-pyr}$) have been interpreted to result from a larger marine sulfate reservoir, as well as complex sulfur cycling associated with oxidative side of the S cycle, both of which are associated with higher oxygen levels. At modern marine sulfate concentrations, the δ^{34}S of seawater should be globally homogeneous and is preserved in carbonate rocks and evaporites.

Sedimentary records show a progressive increase in $\Delta^{34}S_{SO4-pyr}$ across the Ediacaran (635 to approximately 550 Ma) [8], interpreted to represent an increase in the marine sulfate reservoir, and then the onset of oxidative sulfur cycling. The $\Delta^{34}S_{SO4-pyr}$ decreases again in the latest Ediacaran (approx. 550 Ma), along with an increase in $\delta^{34}S_{SO4}$, suggesting increased pyrite burial and a return to anoxia [50]. However, subsequent work has questioned the link between $\Delta^{34}S_{SO4-pyr}$ and oxidative sulfur cycling [51]. A series of rapid oscillations in $\delta^{34}S_{SO4}$ are recorded 524–512 Ma [16], coincident with excursions in $\delta^{13}C_{carb}$, where the rising limbs are associated with periods of ocean anoxia and increased pyrite burial. This increase in net pyrite burial would produce a pulse of

atmospheric oxygen, in turn driving anoxia from the shelf. Further $\delta^{34}S_{SO4}$ oscillations are recorded at around 500 Ma [44]. Sulfur isotopes therefore support dynamic redox conditions into the Cambrian and beyond.

2.3. Constraints on atmospheric oxygen

2.3.1. Chromium isotopes

The oxidation and reduction of Cr between Cr(III) and Cr(IV) result in large fractionations. Cr oxidation occurs through dissolution of Cr(III) in soils and reaction with Mn oxides, the presence of which is linked to free O_2. This yields dissolved Cr(VI) species (CrO_4^{2-} and $HCrO_4^-$) that are more soluble and enriched in the heavy isotope, compared with Cr(III). Therefore, under reducing conditions, the marine Cr record in shales and ironstones will be dominated by unfractionated crustal Cr(III), whereas under an oxidizing atmosphere, the Cr record will be isotopically enriched.

The long-term $\delta^{53}Cr$ record shows a marked enrichment between 800 and 750 Ma [11], recorded in both shales and ironstones, and interpreted to indicate a rise in atmospheric O_2 levels. Although the pre-800 record is dominated by low $\delta^{53}Cr$, isolated examples of ^{53}Cr enrichments have been recorded [52]. Cr(III) oxidation during weathering is dependent on Mn oxide availability. Quantitative modelling suggests Mn oxide formation occurs at low O_2 (greater than 0.1–1% present atmospheric levels (PAL)), providing a maximum constraint on the pre-800 Ma atmosphere [11] and suggesting a modest increase in atmospheric O_2 around 800–750 Ma.

2.3.2. Wildfire record

Wildfires can only be sustained when atmospheric oxygen levels are high (greater than 15–17%) [53]. Charcoal, the geological expression of palaeo-wildfires, is present in the geological record from the latest Silurian onwards [54]. Charcoal is low in abundance across the Silurian and Devonian, but increases by 1–2 orders of magnitude in the late Devonian [55]. This suggests oxygen crossed a critical threshold in the Late Silurian (greater than 15%), but rose further in the Late Devonian (greater than 17%). Wildfires are dependent on the presence of land plants, which evolved approximately 470 Ma, so the charcoal record cannot constrain pre-Ordovician pO_2.

3. Reconciling proxy records

Direct proxies for atmospheric oxygen are scarce. Chromium isotopic fractionations indicate that O_2 rose above 0.1–1% PAL at around 800 Ma [11]; however, earlier evidence for fractionation of chromium has been recorded [52]. More certain is a rise in O_2 to greater than 70% PAL during the Late Silurian and a final rise towards modern levels in the Devonian (greater than 80% PAL or above) [55,56]. Regardless of atmospheric oxygen concentrations, substantial spatial and temporal variability is expected in marine redox conditions, as water column O_2 is controlled by a balance between the oxygen supply and its utilization during remineralization. Modelling calculations suggest that widespread deep ocean oxygenation requires atmospheric oxygen to exceed 30–40% PAL, but this depends on the availability of the limiting nutrient phosphate [57], and on the model itself. That said, to first order, deep water oxygenation would be expected to track a substantial rise in atmospheric oxygen levels.

Some global marine geochemical proxies record a permanent change towards widespread oxygenation in the late Palaeozoic, including $\delta^{98}Mo$ and U enrichments [7,14,46]. Similarly, compilations of local marine redox proxies do not detect any statistically significant change in oxygen availability across the Neoproterozoic, and instead pinpoint widespread marine oxygenation later, in the Late Palaeozoic–Mesozoic: post-Ordovician for Fe speciation [14], Late Devonian for Ce anomalies [29], Late Palaeozoic for $Fe^{3+}/\sum Fe$ ratios [15] and Early Devonian for I/Ca [10]. There is some variability in the precise timing recorded by each proxy, which may be accounted for by their different sensitivity to the spatial extent or location of anoxia, or to increasing redox state. More importantly, the timing of oxygenation in long-term data compilations is highly sensitive to sampling density as well as the boundaries of data bins. For example, $Fe^{3+}/\sum Fe$ ratio data are necessarily sparse as they are derived from rare ophiolites. Therefore, these techniques can only be used to make broad comparisons between, for example, the Early Palaeozoic and Late Palaeozoic. Four compilations of local proxy data, re-analysed using consistent time bins, all show a significant increase in oxygenation in the period 420–250 Ma compared with 580–420 Ma (figure 2).

Broadly anoxic Neoproterozoic–Early Palaeozoic oceans could manifest as oxic surface waters overlying fully anoxic deep waters in a 'pancake' structure (figure 3*a*), or as shallow, expanded OMZs (figure 3*b* and *c*). A four-dimensional transect of local redox conditions across a shelf suggests that OMZ-like structures were established by the Cambrian [58], implying that the deep ocean contained low levels of oxygen. This is consistent with $Fe^{3+}/\sum Fe$ ratios [15] and the marine red bed record [13], which support low levels of oxygen in deep waters from the mid-Ediacaran onwards. A shallower OMZ could be a reflection of lower atmospheric oxygen levels, but could also result from differences in carbon cycling.

If there were indeed mildly oxidizing conditions in the Neoproterozoic–Early Palaeozoic ocean, then how do we reconcile this with global redox proxies that suggest widespread marine anoxia? Global redox proxies tend to record the percentage of seafloor, globally, that is overlain by anoxic bottom waters, but do not provide insight into the location of those anoxic waters. This is further complicated by the lack of information available on marine productivity, sinking fluxes and ocean circulation, which are key controls on OMZ characteristics. Shallowing of OMZs can result in a much larger contact area between anoxic waters and the continental shelf, translating into a larger area of anoxic seafloor, despite no change in the thickness of the OMZ [59] (figure 3*c*,*d*). If the OMZ also expanded in thickness, the combined effect could result in the estimated 10–30% seafloor anoxia and 1% seafloor euxinia required to generate anoxic $\delta^{98}Mo$, $\delta^{238}U$ and U-enrichment signals (figure 3*b*). Furthermore, if bottom waters in the deep ocean were oxic, but contained only low levels of oxygen (less than 10 µM), then shallow pore waters would be commonly driven anoxic, which may further contribute to anoxic draw down of RSE such as Mo and U.

Although large areas of the seafloor remained anoxic or contained only low levels of oxygen through the Neoproterozoic–Lower Palaeozoic, some proxy systems suggest conditions were dynamic, with brief ocean oxygenation

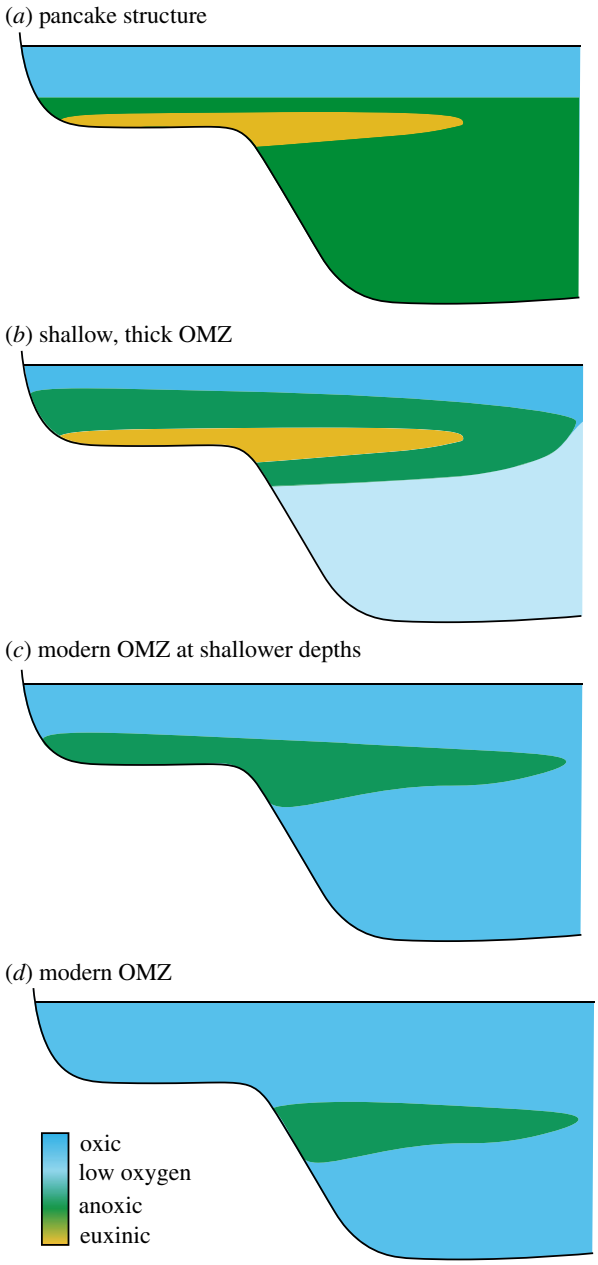

Figure 3. Cartoon showing various possible redox structures for early oceans.

events (OOEs). Some OOEs are recorded independently by multiple proxy systems. For example, the transition back towards anoxic conditions following the 550 Ma OOE is recorded by δ^{98}Mo, δ^{238}U, RSE enrichments, I/Ca ratios and δ^{34}S (figure 1) [8,9,17,18,26,50]. By contrast, OOEs are not detected in any compilations of local proxy data. For I/Ca ratio and Ce anomaly data, this is likely because sample coverage is too sparse to detect them. For Fe speciation or $Fe^{3+}/\sum Fe$ ratio data, OOEs would not be detected as data are binned into periods orders of magnitude longer than the duration of OOEs, so OOEs are averaged out or not sampled. Therefore, global redox proxies, analysed in continuous, high-resolution sections, detect variability that can be missed by compilations of local redox proxies.

4. Modelling the long-term redox transition

Global biogeochemical models can be used to evaluate the processes which have caused the observed oxygenation pattern. The COPSE model [60] is a non-dimensional system (or 'box model'), which computes the operation of the global C-O-P-S cycles over geological timescales and is based on the pioneering GEOCARB models [61,62]. Like GEOCARB, the key considerations for COPSE are the global weathering, burial and degassing processes that control the transfer of key species between the hydrosphere and the crust. The long-term O_2 sources are burial of either organic carbon or pyrite sulfur in sediments (removal of a reductant leads to net oxygenation), and the O_2 sinks are the uplift and weathering, or subduction and degassing, of these reduced species which consumes O_2. Importantly, COPSE differs from the GEOCARB models in that it is a 'forwards' model, meaning that it computes all processes via an internally consistent set of biogeochemical rules [63,64], rather than seeking to infer them directly from the geological record. This means that COPSE can produce estimates of key geochemical proxies such as carbonate $\delta^{13}C$, sulfate $\delta^{34}S$ and strontium $^{87}Sr/^{86}Sr$, which are then used to test the 'skill' of the model by comparing to geological data.

The model is subject to 'external forcings': the rate of tectonic CO_2 input, continental uplift and palaeogeography, exposed lithological classes, and a variety of switches that represent the evolution of different modes of life which affect global biogeochemistry. Recent reviews are available that describe the latest version of the model [65,66]. Originally COPSE was built for reconstructing the Phanerozoic Earth system, but in the last decade, there may have been extensions to apply the model to the late Precambrian. These extensions have tended to focus on single events such as snowball Earth termination [67] or the Shuram negative carbon isotope excursion [68]. We now bring together the key modifications of the model to produce a complete suite of simulations over the Neoproterozoic and Palaeozoic (see electronic supplementary material for full explanation of model parameters and differential equations).

We begin from the model of Mills *et al*. [66], which extended the latest major model release [65] by updating the rates of CO_2 degassing and tectonic uplift with new estimates, as well as revising the link between global climate and chemical weathering rates, informed by Phanerozoic temperature and CO_2 proxies. We then add a function for the evolution of bioturbation during the early Cambrian [69]; a function that represents input of reduced species from the mantle [70]; a deep ocean reservoir of dissolved organic carbon [68]; and an uplift-weathering event of evaporite sulfate coincident with the Shuram negative carbon isotope anomaly [68]. Each of these additions has been made to the model previously in isolation and the reader is referred to the cited work for more details. To summarize: bioturbating animals are assumed to evolve by 520 Ma and are presumed to increase the re-oxidation of sedimentary organic matter and drawdown of the nutrient phosphorus; reductant input is assumed to scale with the ridge generation rate and consumes O_2; a deep ocean reservoir of dissolved organic carbon (DOC) is assumed to have built up over the Precambrian and is rapidly oxidized when the deep ocean becomes oxic—driving a sharp negative carbon isotope excursion; and a large sulfate input event occurs at 580 Ma due to the uplift and weathering of Tonian-age evaporite giants. Debate continues about whether an enlarged marine DOC reservoir is required in order to explain Neoproterozoic C isotope dynamics [71] and around the timing of the effects of bioturbation [72]. It is hoped that further analytical and modelling efforts will help to fully resolve

these questions. Incorporating these mechanisms into a single consistent model is a part of this process.

Figure 1 shows the combined COPSE model predictions for atmospheric O_2 and seafloor anoxia over the Neoproterozoic and Palaeozoic and compares them to the proxies discussed earlier. The brown shaded area represents the boundaries of a suite of 10 000 model sensitivity analyses in which the major external forcings (uplift, degassing, lithology) are varied by ±20%. There is some agreement with the proxies for atmospheric O_2: COPSE predicts (far) above 0.1% PAL for the entire Neoproterozoic, a rise to greater than 70% PAL by the Silurian, and to 100% PAL in the Devonian. This broad pattern is controlled by the evolution of land plants, which are assumed to increase the weathering delivery of the nutrient phosphate (which drives marine productivity), and also the burial of terrestrially derived organic carbon [55]. Other key features of the atmospheric O_2 predictions are a spike between 580 and 570 Ma, caused by uplift and weathering of evaporite sulfate which stimulates pyrite burial [68], and a drop during the Cambrian coincident with the evolution of significant bioturbation, which limits organic carbon preservation [69]. The only area of substantial disagreement with proxies is that COPSE does not produce lower atmospheric O_2 before approximately 800 Ma, whereas the lack of fractionation in the chromium isotope record suggests O_2 might be below 1% PAL [11]. It is not currently clear how strong the constraint from the Cr isotope record is, given that fractionations have been found in several pre-800 Ma samples [52], but it is also possible that a major process is still missing from COPSE, which if included, would result in lower atmospheric O_2. There are several candidates here, including the lack of explicit productivity-remineralization dynamics in the ocean, or a better representation of Precambrian tectonics. Research is ongoing.

The seafloor anoxia prediction from COPSE follows the transitions in atmospheric O_2, with more than 50% of the seafloor anoxic during the Neoproterozoic, and full ventilation during the Devonian. In general agreement with the proxies, there is a period of expanded oxic seafloor immediately post-Gaskiers, which then returns to almost entirely anoxic by the later Cambrian. But there are three major discrepancies between the model predictions and the proxies for seafloor anoxia. First, the model does not produce any of the rapid variability attested to by the proxies (OOEs). Second, the model fails to reproduce longer term oxygenation surrounding the Sturtian and Marinoan glaciations. Finally, the model predicts very large anoxic seafloor areas during the later Cambrian and Ordovician, which are not directly supported by any proxies.

The inability of the COPSE model to reproduce the OOEs in the later Ediacaran and Cambrian is probably due to the model's use of a single-box ocean. In COPSE, the shelf environments and (much more vast) deeper ocean are considered to be a single system. This adds a huge amount of buffering capacity, which may not be realistic. A more sophisticated biogeochemical model [73,74] splits the ocean into multiple boxes representing areas of the shelf, open ocean and deep ocean. This model shows that OOEs can occur due to feedbacks between the marginal phosphorus and oxygen cycles, and thus the lack of OOEs in COPSE may be a consequence of limited representation of shelf environments.

The lack of any appreciable oxygen changes around the Sturtian and Marinoan glaciations is also relatively easily explained, as this version of the COPSE model still does not incorporate any of the processes associated with either the initiation or termination of these snowball Earth events. Looking to the model outputs for sedimentary isotope ratios (figure 4), it is clear that while the post-Gaskiers predictions are within reason, the model is missing major aspects of Earth system function pre-600 Ma, especially in the carbon cycle. Here, the large and sustained positive carbon isotope excursions that occur before the Sturtian, and during the aftermath of both glaciations, may represent increased productivity and oxygen production, which is supported by the O_2 proxies.

An argument could be made that the break-up of the Rodinia supercontinent was underway by approximately 750 Ma [75] and led to enhanced continental weathering [76], high rates of organic carbon burial and high $\delta^{13}C$, before driving the system towards the Sturtian snowball Earth. It is then possible that CO_2 rose to extremely high levels during the glaciations, meaning that the super-greenhouse period that followed glaciation lasted several tens of millions of years before CO_2 could be reduced to background levels [67]. Adding these ideas into the COPSE model is possible, but in order to reproduce the timing of isotope excursions, the weathering response to temperature and the effect of erosion on weathering must be very carefully chosen. Thus, we defer further investigation of the dynamics and timing of global glaciations and weathering events in the Cryogenian to spatial models with a better approximation of continental weathering (e.g. GEOCLIM [77,78]).

The large areas of anoxic seafloor during the Cambrian–Ordovician coincide with carbonate $\delta^{13}C$ predictions that sit generally below the data, indicating that the model may be underestimating oxygen production (or incorrectly simulating organic C weathering [79]). This may be due to an overestimate of the importance of bioturbation in re-oxidizing sedimentary organic carbon and burying phosphate. New reaction–transport models of the bioturbation process will hopefully help test this.

5. Assessing the role of oxygen in early animal evolution

The hypothesized rise in oxygen levels across the Neoproterozoic–Palaeozoic has been repeatedly linked to the origin and radiation of early animals [5–7,11,16,80]. Given that oxygen is required by all extant animals, this hypothesis seems intuitive and has proved rather attractive. But a large body of recent work has shown that the role of oxygen in early animal ecosystems is more complex than previously thought [18,81,82]. One issue is that not all geochemical data provide the information needed to address ecologically relevant questions, such as the precise oxygen levels. Waters containing 100 µM or 1 µM O_2 would be indistinguishable in many proxy systems, but the first could host a complex ecosystem containing skeletal animals and motile predators, and the second would be largely uninhabitable [83,84]. These issues can be partly resolved by considering the systematics of each geochemical proxy, and exactly what information they provide about the redox structure of ancient environments.

Minimum oxygen levels are necessary, but not sufficient, to explain the appearance of new species or ecological traits. Simple sponge-grade animals have very low oxygen demands (1–10 µM) [81], and these requirements appear to have been

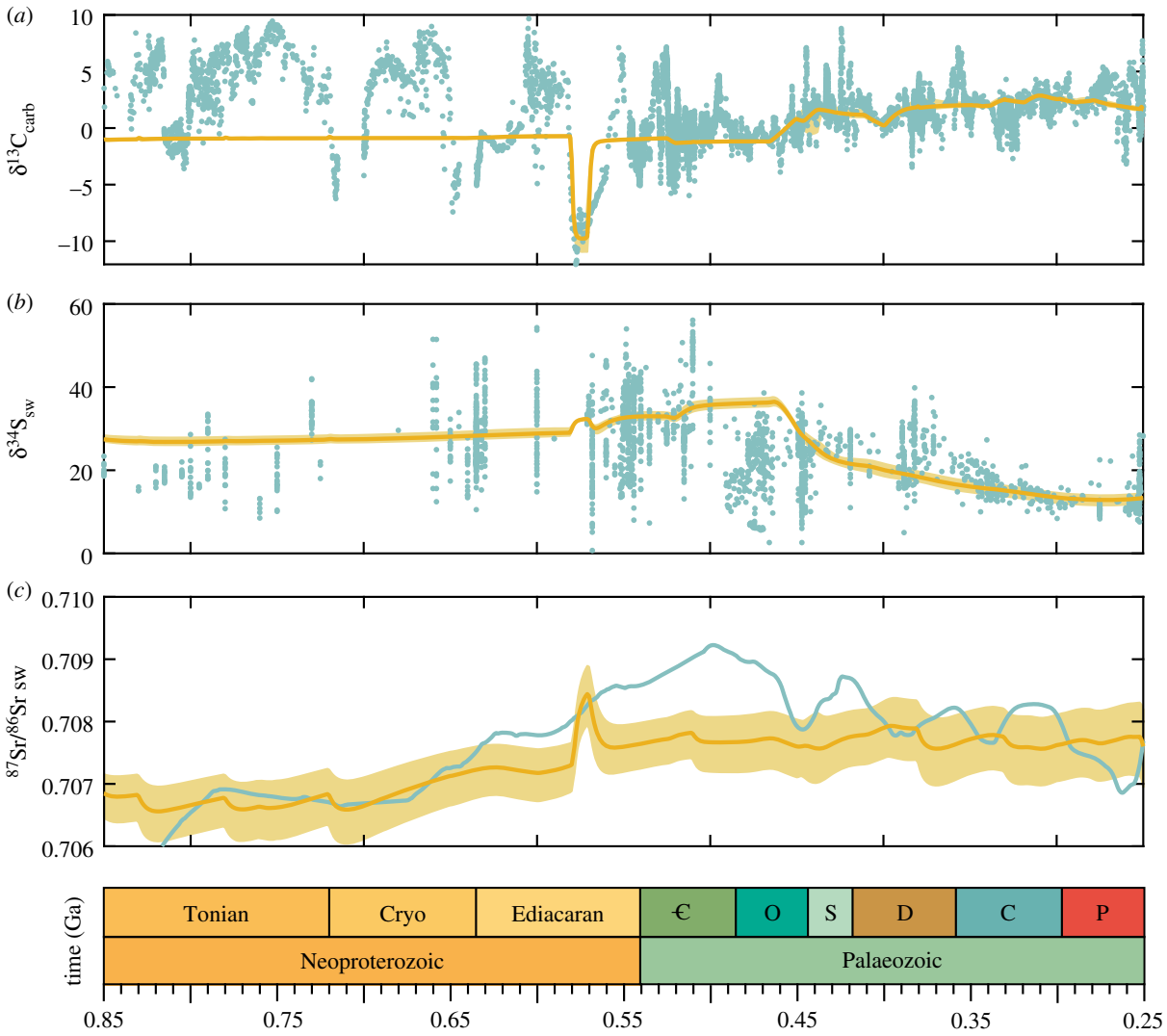

Figure 4. COPSE model isotopic outputs. Geochemical constraints are shown in teal and model outputs in yellow. (*a*) $\delta^{13}C$ carbonate sediments. (*b*) $\delta^{34}S$ seawater sulfate. (*c*) $^{87}Sr/^{86}Sr$ carbonate sediments.

met continuously in surface waters from at least 800 Ma onwards [11]. During the Neoproterozoic, there may have been progressive increase in the maximum dissolved O_2, enabling the development of more aerobically demanding traits, such as motility and bioturbation. However, for most of the Ediacaran, many proxies suggest widespread anoxic deep waters [18,19]. Ecosystem dynamics, animal distributions and migration patterns will be influenced by this reduction in habitable space, but clearly, early animal communities continued to thrive in shallow, well-oxygenated shelf environments where their oxygen demands were met [25,31]. It is therefore important to constrain the maximum $O_2(aq)$ available in shelf environments, as well as the spatial extent of inhospitable environments.

The marine redox landscape in the Cryogenian and Ediacaran appears to have been highly dynamic. It has been suggested that OOEs could have stimulated evolution, and their frequency appears to increase in the late Ediacaran and Cambrian, coincident with an intense period of diversification [17]. Periods of anoxia in between OOEs could even stimulate the development of genetic diversity [82]. Geochemical data and model results suggest that although the Neoproterozoic redox landscape was dynamic, there was no permanent change towards stable, well-oxygenated oceans until at least the Devonian, likely assisted by the evolution of land plants [7,10,14,15,29,55].

6. Conclusion and future directions

The proxy data are best reconciled in the following way: atmospheric O_2 reached a concentration of greater than 0.1% PAL by around approximately 800 Ma and potentially earlier. Surface waters in contact with this atmosphere contained low levels of dissolved oxygen, but the deep oceans remained anoxic. Atmospheric oxygen probably rose in steps or pulses throughout the Cryogenian and Ediacaran, associated with major events such as the break-up of Rodinia, and the Sturtian, Marinoan and Gaskiers glaciations. The post-Sturtian is also marked by the first brief OOEs, which continue into the Cambrian. There is some evidence for OOE magnitude increasing over time [6], and a gradual rise in oxygen over the Neoproterozoic is also consistent with selenium isotope data [12]. By the start of the Cambrian, pO_2 surpassed 30–40% PAL, but oxygen concentrations in much of the deep ocean remained low and the OMZ was thick and shallow. Atmospheric oxygen rose again in the Late Silurian, surpassing 70% PAL, and rose to modern-like levels in the Devonian, pushing

the OMZ back off the shelf and establishing modern, well-oxygenated oceans (figure 3*d*). The COPSE model is unable to reproduce the full complexity revealed by geochemical data, but does capture first-order patterns of atmospheric and marine oxygenation from the Ediacaran onwards, giving confidence that the behaviour we see in the proxies is reasonable. The hypothesized NOE would be more accurately described as a Neoproterozoic Oxygenation Window, featuring dynamic pulses of oxygenation against a background of gradually rising oxygen levels, and any step change towards stable, well-oxygenated conditions appears to have been delayed until the Palaeozoic Oxygenation Event.

Moving forward, we need to consider which geochemical data can best capture this transition. To understand the timing, frequency and duration of OOEs, we need to target high-resolution continuous successions and analyse multiple global redox proxies. To meaningfully address questions surrounding the role of oxygen in early animal ecosystems, we need to focus on developing quantitative constraints on maximum $O_2(aq)$. These could include proxies for atmospheric oxygen, such as Cr isotopes, or marine redox proxies that respond to intermediate redox conditions, such as Ce anomalies and I/Ca. Detailed four-dimensional maps across shelf ecosystems can reveal the structure of marine anoxia (i.e. pancake versus OMZ) and be tied directly to the fossil record.

Data accessibility. The geochemical data are all published elsewhere and discussed in full in the relevant references. Differential equations and fixed parameters from the model are available in the electronic supplementary material. All modelling code and outputs can be obtained from B.J.W.M. on request.

Authors' contributions. R.T. compiled proxy data, and B.J.W.M. modified the COPSE biogeochemical model. R.T. and B.J.W.M discussed the results and wrote the manuscript together.

Competing interests. The authors declare no competing interests.

Funding. R.T. is supported by a grant from the DSI-NRF Centre of Excellence in Palaeosciences and B.J.W.M is funded by the UK Natural Environment Research Council (NE/R010129/1 and NE/S009663/1) and by a University of Leeds Academic Fellowship.

Acknowledgements. We are grateful to Zunli Lu and Noah Planavsky for reviews that helped to improve the manuscript. We thank the Royal Society for supporting us to attend a meeting in London where these ideas were discussed.

References

1. Farquhar J, Bao H, Thiemens M. 2000 Atmospheric influence of Earth's earliest sulfur cycle. *Science* **289**, 756–758. (doi:10.1126/science.289.5480.756)
2. Och LM, Shields-Zhou GA. 2012 The Neoproterozoic oxygenation event: environmental perturbations and biogeochemical cycling. *Earth-Sci. Rev.* **110**, 26–57. (doi:10.1016/j.earscirev.2011.09.004)
3. Scott C, Lyons TW, Bekker A, Shen Y, Poulton SW, Chu X, Anbar AD. 2008 Tracing the stepwise oxygenation of the Proterozoic ocean. *Nature* **452**, 456–459. (doi:10.1038/nature06811)
4. Canfield DE, Farquhar J. 2009 Animal evolution, bioturbation, and the sulfate concentration of the oceans. *Proc. Natl Acad. Sci. USA* **106**, 8123–8127. (doi:10.1073/pnas.0902037106)
5. Canfield DE, Poulton SW, Narbonne GM. 2007 Late-Neoproterozoic deep-ocean oxygenation and the rise of animal life. *Science* **315**, 92–95. (doi:10.1126/science.1135013)
6. Chen X *et al.* 2015 Rise to modern levels of ocean oxygenation coincided with the Cambrian radiation of animals. *Nat. Commun.* **6**, 7142. (doi:10.1038/ncomms8142)
7. Dahl TW *et al.* 2010 Devonian rise in atmospheric oxygen correlated to the radiations of terrestrial plants and large predatory fish. *Proc. Natl Acad. Sci. USA* **107**, 17 911–17 915. (doi:10.1073/pnas.1011287107)
8. Fike DA, Grotzinger JP, Pratt LM, Summons RE. 2006 Oxidation of the Ediacaran ocean. *Nature* **444**, 744–747. (doi:10.1038/nature05345)
9. Kendall B *et al.* 2015 Uranium and molybdenum isotope evidence for an episode of widespread ocean oxygenation during the late Ediacaran Period. *Geochim. Cosmochim. Acta* **156**, 173–193. (doi:10.1016/j.gca.2015.02.025)
10. Lu W *et al.* 2018 Late inception of a resiliently oxygenated upper ocean. *Science* **361**, 174–177. (doi:10.1126/science.aar5372)
11. Planavsky NJ, Reinhard CT, Wang X, Thomson D, Mcgoldrick P, Rainbird RH, Johnson T, Fischer WW, Lyons TW. 2014 Low Mid-Proterozoic atmospheric oxygen levels and the delayed rise of animals. *Science* **346**, 635–638. (doi:10.1126/science.1258410)
12. von Strandmann P, Stüeken EE, Elliott T, Poulton SW, Dehler CM, Canfield DE, Catling DC. 2015 Selenium isotope evidence for progressive oxidation of the Neoproterozoic biosphere. *Nat. Commun.* **6**, 10157. (doi:10.1038/ncomms10157)
13. Song H *et al.* 2017 The onset of widespread marine red beds and the evolution of ferruginous oceans. *Nat. Commun.* **8**, 399. (doi:10.1038/s41467-017-00502-x)
14. Sperling EA *et al.* 2015 Statistical analysis of iron geochemical data suggests limited late Proterozoic oxygenation. *Nature* **523**, 451–454. (doi:10.1038/nature14589)
15. Stolper DA, Keller CB. 2018 A record of deep-ocean dissolved O_2 from the oxidation state of iron in submarine basalts. *Nature* **553**, 323–327. (doi:10.1038/nature25009)
16. He T *et al.* 2019 Possible links between extreme oxygen perturbations and the Cambrian radiation of animals. *Nat. Geosci.* **12**, 468–474. (doi:10.1038/s41561-019-0357-z)
17. Sahoo SK, Planavsky NJ, Jiang G, Kendall B, Owens JD, Wang X, Shi X, Anbar AD, Lyons TW. 2016 Oceanic oxygenation events in the anoxic Ediacaran ocean. *Geobiology* **14**, 457–468. (doi:10.1111/gbi.12182)
18. Tostevin R, Clarkson MO, Gangl S, Shields GA, Wood RA, Bowyer F, Penny AM, Stirling CH. 2019 Uranium isotope evidence for an expansion of anoxia in terminal Ediacaran oceans. *Earth Planet. Sci. Lett.* **506**, 104–112. (doi:10.1016/j.epsl.2018.10.045)
19. Zhang F, Xiao S, Kendall B, Romaniello SJ, Cui H, Meyer M, Gilleaudeau GJ, Kaufman AJ, Anbar AD. 2018 Extensive marine anoxia during the terminal Ediacaran Period. *Sci. Adv.* **4**, eaan8983. (doi:10.1126/sciadv.aan8983)
20. Kurzweil F, Drost K, Pašava J, Wille M, Taubald H, Schoeckle D, Schoenberg R. 2015 Coupled sulfur, iron and molybdenum isotope data from black shales of the Teplá-Barrandian unit argue against deep ocean oxygenation during the Ediacaran. *Geochim. Cosmochim. Acta* **171**, 121–142. (doi:10.1016/j.gca.2015.08.022)
21. Johnston DT, Poulton SW, Tosca NJ, O'brien T, Halverson GP, Schrag DP, Macdonald FA. 2013 Searching for an oxygenation event in the fossiliferous Ediacaran of northwestern Canada. *Chem. Geol.* **362**, 273–286. (doi:10.1016/j.chemgeo.2013.08.046)
22. Ling H-F, Chen X, Li D, Wang D, Shields-Zhou GA, Zhu M. 2013 Cerium anomaly variations in Ediacaran–earliest Cambrian carbonates from the Yangtze Gorges area, South China: implications for oxygenation of coeval shallow seawater. *Precambrian Res.* **225**, 110–127. (doi:10.1016/j.precamres.2011.10.011)
23. Poulton SW, Canfield DE. 2005 Development of a sequential extraction procedure for iron: implications for iron partitioning in continentally derived particulates. *Chem. Geol.* **214**, 209–221. (doi:10.1016/j.chemgeo.2004.09.003)
24. Canfield DE, Poulton SW, Knoll AH, Narbonne GM, Ross G, Goldberg T, Strauss H. 2008 Ferruginous conditions dominated later Neoproterozoic deep-water chemistry. *Science* **321**, 949–952. (doi:10.1126/science.1154499)

25. Wood RA *et al.* 2015 Dynamic redox conditions control late Ediacaran ecosystems in the Nama Group, Namibia. *Precambrian Res.* **261**, 252–271. (doi:10.1016/j.precamres.2015.02.004)
26. Hardisty DS *et al.* 2017 Perspectives on Proterozoic surface ocean redox from iodine contents in ancient and recent carbonate. *Earth Planet. Sci. Lett.* **463**, 159–170. (doi:10.1016/j.epsl.2017.01.032)
27. Uahengo C-I, Shi X, Jiang G, Vatuva A. 2020 Transient shallow-ocean oxidation associated with the late Ediacaran Nama skeletal fauna: evidence from iodine contents of the Lower Nama Group, southern Namibia. *Precambrian Res.* **343**, 105732. (doi:10.1016/j.precamres.2020.105732)
28. Lu W, Wörndle S, Halverson GP, Zhou X, Bekker A, Rainbird RH, Hardisty DS, Lyons TW, Lu Z. 2017 Iodine proxy evidence for increased ocean oxygenation during the Bitter Springs Anomaly. *Geochem. Perspect. Lett.* **5**, 53–57. (doi:10.7185/geochemlet.1746)
29. Wallace MW, Hood AS, Shuster A, Greig A, Planavsky NJ, Reed CP. 2017 Oxygenation history of the Neoproterozoic to early Phanerozoic and the rise of land plants. *Earth Planet. Sci. Lett.* **466**, 12–19. (doi:10.1016/j.epsl.2017.02.046)
30. Nothdurft LD, Webb GE, Kamber BS. 2004 Rare earth element geochemistry of Late Devonian reefal carbonates, Canning Basin, Western Australia: confirmation of a seawater REE proxy in ancient limestones. *Geochim. Cosmochim. Acta* **68**, 263–283. (doi:10.1016/S0016-7037(03)00422-8)
31. Tostevin R *et al.* 2016 Low-oxygen waters limited habitable space for early animals. *Nat. Commun.* **7**, 12818. (doi:10.1038/ncomms12818)
32. Boyer DL, Owens JD, Lyons TW, Droser ML. 2011 Joining forces: combined biological and geochemical proxies reveal a complex but refined high-resolution palaeo-oxygen history in Devonian epeiric seas. *Palaeogeogr. Palaeoclimatol. Palaeoecol.* **306**, 134–146. (doi:10.1016/j.palaeo.2011.04.012)
33. Lu W, Dickson AJ, Thomas E, Rickaby REM, Chapman P, Lu Z. In press. Refining the planktic foraminiferal I/Ca proxy: results from the southeast Atlantic Ocean. *Geochim. Cosmochim. Acta*. (doi:10.1016/j.gca.2019.10.025)
34. Macdonald FA, Strauss JV, Sperling EA, Halverson GP, Narbonne GM, Johnston DT, Kunzmann M, Schrag DP, Higgins JA. 2013 The stratigraphic relationship between the Shuram carbon isotope excursion, the oxygenation of Neoproterozoic oceans, and the first appearance of the Ediacara biota and bilaterian trace fossils in northwestern Canada. *Chem. Geol.* **362**, 250–272. (doi:10.1016/j.chemgeo.2013.05.032)
35. De Carlo EH, Green WJ. 2002 Rare earth elements in the water column of Lake Vanda, McMurdo Dry Valleys, Antarctica. *Geochim. Cosmochim. Acta* **66**, 1323–1333. (doi:10.1016/S0016-7037(01)00861-4)
36. O'Connell B, Wallace MW, Hood AvS, Lechte MA, Planavsky NJ. 2020 Iron-rich carbonate tidal deposits, Angepena Formation, South Australia: a redox-stratified Cryogenian basin. *Precambrian Res.* **342**, 105668. (doi:10.1016/j.precamres.2020.105668)
37. Banner JL, Hanson GN, Meyers WJ. 1988 Rare earth element and Nd isotopic variations in regionally extensive dolomites from the Burlington-Keokuk formation (Mississippian): implications for REE mobility during carbonate diagenesis. *J. Sediment. Res.* **58**, 415–432. (doi:10.2110/jsr.58.673)
38. Lau KV, RomanielloSJ, Zhang F. 2019 The uranium isotope paleoredox proxy. In *Elements in geochemical tracers in earth system science*. Cambridge, UK: Cambridge University Press. (doi:10.1017/9781108584142)
39. Rolison JM, Stirling CH, Middag R, Rijkenberg MJA. 2017 Uranium stable isotope fractionation in the Black Sea: modern calibration of the $^{238}U/^{235}U$ paleo-redox proxy. *Geochim. Cosmochim. Acta* **203**, 69–88. (doi:10.1016/j.gca.2016.12.014)
40. Lau KV, Macdonald FA, Maher K, Payne JL. 2017 Uranium isotope evidence for temporary ocean oxygenation in the aftermath of the Sturtian Snowball Earth. *Earth Planet. Sci. Lett.* **458**, 282–292. (doi:10.1016/j.epsl.2016.10.043)
41. Chen X, Romaniello SJ, Herrmann AD, Hardisty D, Gill BC, Anbar AD. 2018 Diagenetic effects on uranium isotope fractionation in carbonate sediments from the Bahamas. *Geochim. Cosmochim. Acta* **237**, 294–311. (doi:10.1016/j.gca.2018.06.026)
42. Dahl TW. 2017 Reorganisation of Earth's biogeochemical cycles briefly oxygenated the oceans 520 Myr ago. *Geochem. Perspect. Lett.* **3**, 210–220. (doi:10.7185/geochemlet.1724)
43. Wei G-Y, Planavsky NJ, Tarhan LG, Chen X, Wei W, Li D, Ling H-F. 2018 Marine redox fluctuation as a potential trigger for the Cambrian explosion. *Geology* **46**, 587–590. (doi:10.1130/G40150.1)
44. Dahl TW, Boyle RA, Canfield DE, Connelly JN, Gill BC, Lenton TM, Bizzarro M. 2014 Uranium isotopes distinguish two geochemically distinct stages during the later Cambrian SPICE event. *Earth Planet. Sci. Lett.* **401**, 313–326. (doi:10.1016/j.epsl.2014.05.043)
45. White DA, Elrick M, Romaniello S, Zhang F. 2018 Global seawater redox trends during the Late Devonian mass extinction detected using U isotopes of marine limestones. *Earth Planet. Sci. Lett.* **503**, 68–77. (doi:10.1016/j.epsl.2018.09.020)
46. Partin CA *et al.* 2013 Large-scale fluctuations in Precambrian atmospheric and oceanic oxygen levels from the record of U in shales. *Earth Planet. Sci. Lett.* **369–370**, 284–293. (doi:10.1016/j.epsl.2013.03.031)
47. Reinhard CT, Planavsky NJ, Robbins J, Partin C, Gill BC, Lalonde SV, Bekker A, Konhauser KO, Lyons TW. 2013 Proterozoic ocean redox and biogeochemical stasis. *Proc. Natl Acad. Sci. USA* **110**, 5357–5362. (doi:10.1073/pnas.1208622110)
48. Fernández-Martínez A, Charlet L. 2009 Selenium environmental cycling and bioavailability: a structural chemist point of view. *Rev. Environ. Sci. Biotechnol.* **8**, 81–110. (doi:10.1007/s11157-009-9145-3)
49. Fike DA, Bradley AS, Rose CV. 2015 Rethinking the ancient sulfur cycle. *Annu. Rev. Earth Planet. Sci.* **43**, 593–622. (doi:10.1146/annurev-earth-060313-054802)
50. Ries JB, Fike DA, Pratt LM, Lyons TW, Grotzinger JP. 2009 Superheavy pyrite (δ^{34}Spyr > δ^{34}SCAS) in the terminal Proterozoic Nama Group, southern Namibia: a consequence of low seawater sulfate at the dawn of animal life. *Geology* **37**, 743–746. (doi:10.1130/G25775A.1)
51. Sim MS, Bosak T, Ono S. 2011 Large sulfur isotope fractionation does not require disproportionation. *Science* **333**, 74–77. (doi:10.1126/science.1205103)
52. Canfield DE, Zhang S, Frank AB, Wang X, Wang H, Su J, Ye Y, Frei R. 2018 Highly fractionated chromium isotopes in Mesoproterozoic-aged shales and atmospheric oxygen. *Nat. Commun.* **9**, 2871. (doi:10.1038/s41467-018-05263-9)
53. Belcher CM, McElwain JC. 2008 Limits for combustion in low O_2 redefine Paleoatmospheric predictions for the Mesozoic. *Science* **321**, 1197–1200. (doi:10.1126/science.1160978)
54. Glasspool IJ, Edwards D, Axe L. 2004 Charcoal in the Silurian as evidence for the earliest wildfire. *Geology* **32**, 381–383. (doi:10.1130/G20363.1)
55. Lenton TM Dahl TW, Daines SJ, Mills BJW, Ozaki K, Saltzman MR, Porada P. 2016 Earliest land plants created modern levels of atmospheric oxygen. *Proc. Natl Acad. Sci. USA* **113**, 9704–9709. (doi:10.1073/pnas.1604787113)
56. Glasspool IJ, Scott AC. 2010 Phanerozoic concentrations of atmospheric oxygen reconstructed from sedimentary charcoal. *Nat. Geosci.* **3**, 627–630. (doi:10.1038/ngeo923)
57. Canfield DE. 1998 A new model for Proterozoic ocean chemistry. *Nature* **396**, 450–453. (doi:10.1038/24839)
58. Guilbaud R, Slater BJ, Poulton SW, Harvey THP, Brocks JJ, Nettersheim BJ, Butterfield NJ. 2018 Oxygen minimum zones in the early Cambrian ocean. *Geochem. Perspect. Lett.* **6**, 33–38. (doi:10.7185/geochemlet.1806)
59. Lau KV *et al.* 2016 Marine anoxia and delayed Earth system recovery after the end-Permian extinction. *Proc. Natl Acad. Sci. USA* **113**, 2360–2365. (doi:10.1073/pnas.1515080113)
60. Bergman NM, Lenton TM, Watson AJ. 2004 COPSE: a new model of biogeochemical cycling over Phanerozoic time. *Am. J. Sci.* **304**, 397–437. (doi:10.2475/ajs.304.5.397)
61. Berner RA. 1994 GEOCARB II: a revised model of atmospheric CO_2 over Phanerozoic time. *Am. J. Sci.* **294**, 56–91. (doi:10.2475/ajs.294.1.56)
62. Berner RA. 1991 A model for atmospheric CO_2 over Phanerozoic time. *Am. J. Sci.* **291**, 339–376. (doi:10.2475/ajs.291.4.339)
63. Cappellen PV, Ingall ED. 1994 Benthic phosphorus regeneration, net primary production, and ocean anoxia: a model of the coupled marine biogeochemical cycles of carbon and phosphorus. *Paleoceanography* **9**, 677–692. (doi:10.1029/94PA01455)
64. Lenton TM, Watson AJ. 2000 Redfield revisited: 2. What regulates the oxygen content of the

atmosphere? *Glob. Biogeochem. Cycles* **14**, 249–268. (doi:10.1029/1999GB900076)

65. Lenton TM, Daines SJ, Mills BJW. 2018 COPSE reloaded: an improved model of biogeochemical cycling over Phanerozoic time. *Earth-Sci. Rev.* **178**, 1–28. (doi:10.1016/j.earscirev.2017.12.004)
66. Mills BJW, Krause AJ, Scotese CR, Hill DJ, Shields GA, Lenton TM. 2019 Modelling the long-term carbon cycle, atmospheric CO_2, and Earth surface temperature from late Neoproterozoic to present day. *Gondwana Res.* **67**, 172–186. (doi:10.1016/j.gr.2018.12.001)
67. Mills B, Watson AJ, Goldblatt C, Boyle R, Lenton TM. 2011 Timing of Neoproterozoic glaciations linked to transport-limited global weathering. *Nat. Geosci.* **4**, 861–864. (doi:10.1038/ngeo1305)
68. Shields GA, Mills BJW, Zhu M, Raub TD, Daines SJ, Lenton TM. 2019 Unique Neoproterozoic carbon isotope excursions sustained by coupled evaporite dissolution and pyrite burial. *Nat. Geosci.* **12**, 823–827. (doi:10.1038/s41561-019-0434-3)
69. van de Velde S, Mills BJW, Meysman FJR, Lenton TM, Poulton SW. 2018 Early Palaeozoic ocean anoxia and global warming driven by the evolution of shallow burrowing. *Nat. Commun.* **9**, 2554. (doi:10.1038/s41467-018-04973-4)
70. Williams JJ, Mills BJW, Lenton TM. 2019 A tectonically driven Ediacaran oxygenation event. *Nat. Commun.* **10**, 2690. (doi:10.1038/s41467-019-10286-x)
71. Husson JM, Linzmeier BJ, Kitajima K, Ishida A, Maloof AC, Schoene B, Peters SE, Valley JW. 2020 Large isotopic variability at the micron-scale in 'Shuram' excursion carbonates from South Australia. *Earth Planet. Sci. Lett.* **538**, 116211. (doi:10.1016/j.epsl.2020.116211)
72. Tarhan LG. 2018 The early Paleozoic development of bioturbation—evolutionary and geobiological consequences. *Earth-Sci. Rev.* **178**, 177–207. (doi:10.1016/j.earscirev.2018.01.011)
73. Alcott LJ, Mills BJW, Poulton SW. 2019 Stepwise Earth oxygenation is an inherent property of global biogeochemical cycling. *Science* **366**, 1333–1337. (doi:10.1126/science.aax6459)
74. Slomp CP, Van Cappellen P. 2006 The global marine phosphorus cycle: sensitivity to oceanic circulation. *Biogeosci. Discuss.* **3**, 1587–1629. (doi:10.5194/bgd-3-1587-2006)
75. Li ZX *et al.* 2008 Assembly, configuration, and break-up history of Rodinia: a synthesis. *Precambrian Res.* **160**, 179–210. (doi:10.1016/j.precamres.2007.04.021)
76. Donnadieu Y, Goddéris Y, Ramstein G, Nédélec A, Meert J. 2004 A 'snowball Earth' climate triggered by continental break-up through changes in runoff. *Nature* **428**, 303–306. (doi:10.1038/nature02408)
77. Goddéris Y, Donnadieu Y, Carretier S, Aretz M, Dera G, Macouin M, Regard V. 2017 Onset and ending of the late Palaeozoic ice age triggered by tectonically paced rock weathering. *Nat. Geosci.* **10**, 382–386. (doi:10.1038/ngeo2931)
78. Goddéris Y, Donnadieu Y, Le Hir G, Lefebvre V, Nardin E. 2014 The role of palaeogeography in the Phanerozoic history of atmospheric CO_2 and climate. *Earth-Sci. Rev.* **128**, 122–138. (doi:10.1016/j.earscirev.2013.11.004)
79. Daines SJ, Mills BJW, Lenton TM. 2017 Atmospheric oxygen regulation at low Proterozoic levels by incomplete oxidative weathering of sedimentary organic carbon. *Nat. Commun.* **8**, 14379. (doi:10.1038/ncomms14379)
80. Nursall J. 1959 Oxygen as a prerequisite to the origin of the Metazoa. *Nature* **183**, 1170–1172. (doi:10.1038/1831170b0)
81. Mills DB, Ward LM, Jones C, Sweeten B, Forth M, Treusch AH, Canfield DE. 2014 Oxygen requirements of the earliest animals. *Proc. Natl Acad. Sci. USA* **111**, 4168–4172. (doi:10.1073/pnas.1400547111)
82. Wood R, Erwin DH. 2018 Innovation not recovery: dynamic redox promotes metazoan radiations. *Biol. Rev.* **93**, 863–873. (doi:10.1111/brv.12375)
83. Levin LA, Gage JD, Martin C, Lamont PA. 2000 Macrobenthic community structure within and beneath the oxygen minimum zone, NW Arabian Sea. *Deep Sea Res.* **47**, 189–226. (doi:10.1016/S0967-0645(99)00103-4)
84. Sperling EA, Frieder CA, Raman AV, Girguis PR, Levin LA, Knoll AH. 2013 Oxygen, ecology, and the Cambrian radiation of animals. *Proc. Natl Acad. Sci. USA* **110**, 13 446–13 451. (doi:10.1073/pnas.1312778110)